Analyst

Accepted Manuscript

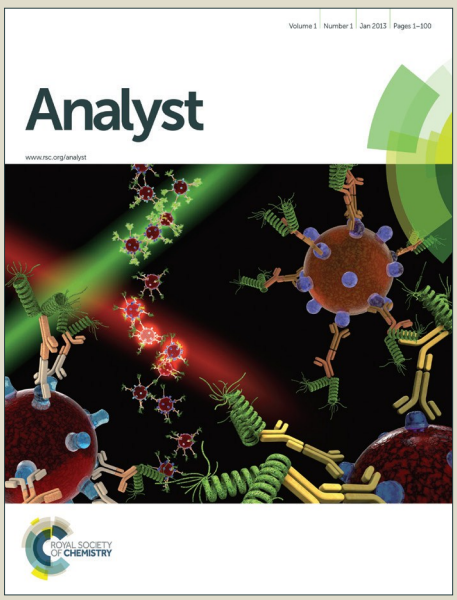

ROYAL SOCIETY OF CHEMISTRY

www.rsc.org/analyst

Comparison of $C_{60}^{+(+)}$ and Ar_n^+ as sputtering ions for SIMS depth profiling of cholesterol thin films.

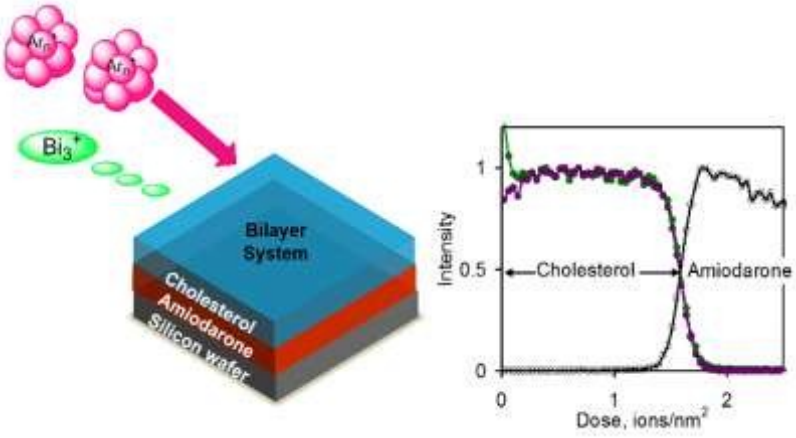

Determination of the Sputtering Yield of Cholesterol Using Ar_n^+ and $C_{60}^{+(+)}$ Cluster Ions

P. D. Rakowska, M. P. Seah, J.-L. Vorng, R. Havelund and I. S. Gilmore

National Physical Laboratory, Hampton Road, Teddington, Middlesex, UK, TW11 0LW

ABSTRACT

The sputtering yield of cholesterol films on silicon wafers is measured using Ar_n^+ and $C_{60}^{+(+)}$ ions in popular energy (E) and cluster size (n) ranges. It is shown that the $C_{60}^{+(+)}$ ions form a surface layer that stabilizes the film so that a well-behaved profile is obtained. On the other hand, the Ar_n^+ gas clusters leave the material very clean but, at room temperature, the layer readily restructures into molecular bilayers, so that, although a useful measure may be made of the sputtering yield, the profiles become much more complex. This restructuring does not occur at room temperature normally but results from the actions of the beams in the sputtering process for profiling in secondary ion mass spectrometry. Better profiles may be made by reducing the sample temperature to -100 °C. This is likely to be necessary for many lower molecular weight materials (below 1000 Da) to avoid the movement of molecules. Measurements for cholesterol films on 37 nm of amiodarone on silicon are even better behaved and show the same sputtering yields at room temperature as those films directly on silicon at -100 °C. The yields for both $C_{60}^{+(+)}$ and Ar_n^+ fit the universal yield equation to a standard deviation of 11%.

Keywords: bilayers, cholesterol, gas clusters, GCIB, organics, restructuring, SIMS, sputtering yields

INTRODUCTION

Cholesterol is one of the most important lipids in the human body. As a key component of nearly all mammalian cell membranes, it is a molecule of a particular interest. It alters the physical properties of the cell membranes, interacts with neighbouring lipids and proteins and is involved in numerous biomolecular processes. It has been proved that cholesterol plays a key role in the regulation of mechanisms such as cell mobility and cell propagation and, therefore presents a crucial factor in cancer metastasis.[1, 2] Cholesterol serves as a precursor for bile salts, vitamin D and steroid hormones.[3] It is also associated to the pathophysiology of various diseases like atherosclerosis[4] or Alzheimer's disease.[5] Consequently, being able to detect, identify and characterize the distribution of cholesterol in biological samples has widespread implications in medical sciences.

Secondary Ion Mass Spectrometry (SIMS) has become an invaluable tool to study organic and biological materials. For depth profiling these materials, the Ar gas cluster ion beam (GCIB)[6] has emerged as the prevailing sputtering source, surpassing the use of the C_{60} ion beam. For example, Rading et al.[7] applied both the sputtering sources to a range of polymer samples, showing that most of the limitations of C_{60} sputtering could be overcome with the use of the Ar clusters, especially for the sputtering of organic materials. Niehuis et al.[8] measured the depth resolution for a range of sizes of Ar clusters for sputtering organic multilayers. The implementation of Ar GCIB ion sources brought great enhancement of the molecular ion yields[9] without significant sample degradation and this opened up the fields of molecular depth profiling and three-dimensional (3D) imaging of samples. With these developments, the number of studies utilising high-resolution imaging and 3D analysis of tissues and cells is rapidly growing and sub-cellular 3D imaging is now possible, as demonstrated recently by Passarelli et al.,[10] who imaged the

disposition of the drug amiodarone within macrophage cells.[10] These experiments are most often performed in the dual beam mode,[11] which has now become a standard operation mode in the analysis of organic and biological samples using time of flight (ToF) SIMS. It encompasses, typically, a high-performance pulsed Bi cluster liquid metal ion gun (LMIG) applied for the analysis of the surface in the centre of the crater sputtered by the Ar clusters. This combines the high lateral and mass resolutions of the LMIG source with the excellent depth profiling of the Ar clusters.[7, 8]

Depth resolution, sputtering yields and secondary ion yields are all important to the quality of the depth profiles and there are many factors that affect these. Operation parameters e.g. primary ion energy, species and angle of incidence[12] as well as chemistry and topography of the sample and the sample handling procedures all influence the experiments and results. Technological developments and a deeper understanding of underlying fundamental processes have led to a rapid growth in the applicability of SIMS imaging to organic and biological materials.[13] In 2013, Seah[14] proposed a generic equation for sputtering yields, *Y*, for argon gas clusters of energy *E* with *n* atoms in the cluster:

$$\frac{Y}{n} = \frac{B[E/(An)]^q}{1 + [E/(An)]^{q-1}} \qquad (1)$$

where the coefficient *B* is unity when the yield is measured in atoms per primary ion and is of the order of 0.01 nm^3 when the yield is measured as a volume in nm^3. It has been found helpful for organic materials, in practice, to measure the yield as a volume – the volume is what is measured directly and it is fairly consistent between organic materials.[14] Equation (1) described the yields of Au, Si, SiO_2, Irganox 1010 ($C_{73}H_{108}O_{12}$ with molecular mass 1176.78 Da), the model organic light emitting diode material HTM-1 (2,2',7,7'-tetra(N,N-ditolyl)amino-9,9-spiro-bifluorene, $C_{81}H_{68}N_4$ with molecular mass 1096.54 Da), polystyrene (PS), polycarbonate (PC) and polymethylmethacrylate (PMMA), as measured in a range of laboratories.[14] These involved energies from 2.5 to 40 keV and cluster sizes from 100 to 10000 atoms. The important parameter, *A*, was found to be high for the elements and inorganic compounds and low for organic and polymeric materials. It was found that *A* was related to *U*, the energy per atom, excluding hydrogen, to remove the fragment from the solid. For elements where most of the fragments are monoatomic, *U* is of the order of 3 to 4 eV but for organic materials with 10 to 20 carbon atoms in typical fragments, this energy is 10 to 20 times smaller and so the value of *A* was that much smaller. The average *A* value for the elements and inorganic materials was ~50 eV and for the polymers and organic materials, ~3 eV. The parameter *q* is also important and was typically ~3. For E/n values less than *A*, equation (1) shows how the yield starts to fall more rapidly with the power dependence being $(E/n)^q$. In practical situations, elemental and inorganic solids are generally in this $E/n < A$ regime whereas polymers and organics, with their lower *A* values, are more in the linear regime where *Y* is approximately proportional to *E*.[14] Seah's study[14] showed how organic materials had yields of 10^4 times those of inorganic materials at E/n values around 1 eV, falling to 100 times for $E/n > 4$ eV. More recent work adds data for NPB[15] (4,4'-bis[N-(1-naphthyl-1-)-N-phenyl-amino]-biphenyl, $C_{44}H_{32}N_2$ with molecular mass 588.75 Da) and both PS and PMMA for a range of molecular weights.[16]

Cholesterol is one of the most easily detectable biomolecules in tissue by SIMS.[17-19] Even if the experiments are not concerned with cholesterol itself, its occurrence in the sample can prove useful. For instance, in brain tissue imaging cholesterol is often used to distinguish different domains in brain sections as it predominantly is detectable in white matter.[20, 21] It has been noted that its presence can provide a chemical enrichment to promote protonation of neighbouring species.[22,23] On the other hand, it can also create a strong matrix effect suppressing the detection of other molecular ions.[21] Also, as shown by Angerer et al.,[21] one must be aware of the susceptibility of cholesterol to migrate during sample handling. In vacuum at temperatures > 0 °C it migrates through tissue to the exposed surface which affects

its apparent distribution in images.[21] Crystal-like structures, in the order of 10 µm long, observed at the surface of tissue sections have been attributed to cholesterol.[21] Other studies have shown that the cholesterol can be completely removed in a prolonged freeze-drying process.[22, 24, 25]

The behaviour of cholesterol during depth profiling and 3D imaging by SIMS has also been studied on model samples including thin films. In a study by Kozole et al.,[26] profiles were made for cholesterol films on Si wafers using 40 keV C_{60}^+ at 40° and 73° incidence angles. The depth profiles are clear with the $[M\text{-}OH]^+$ secondary ion at 369 Da providing good intensity plateaus. For a film of 277 nm thickness, depth resolutions of 32 nm and 19 nm (i.e. 12% and 7%, respectively) were achieved at the two angles. The sputtering yield was determined from atomic force microscopy (AFM) studies to be 503 and 425 molecule equivalents. Using a molecular density of 1.85×10^{21} molecules/cm^3, these results give sputtering yield volumes of 272 and 230 nm^3 at 40° and 73°, respectively.

In the study by Shen et al.,[27] profiles are given for cholesterol layers sputtered by C_{60}^+ at 40 keV. Studies of single layers of 325 and 622 nm thickness showed simple, clear profiles by monitoring the $[M\text{-}OH]^+$ ion at 369 Da and the $[M\text{-}H]^+$ ion at 385 Da, both characteristic of cholesterol. These gave a sputtering yield of 274 ± 20 nm^3 per ion at 40° to the surface normal, in excellent agreement with the result of Kozole et al.[26] In these samples, thin Au layers are also sandwiched between two cholesterol layers on a Si wafer substrate. These show that the sputtering yield of the Au is some 100 times lower than that of cholesterol and that matrix effects significantly alter the ion yields at interfaces. This great disparity of yields is well established for argon cluster sputtering.[14]

Rabani et al.[19] compared the effects of different primary ions: C_{60} and Ar_n^+ (n = 60 – 3000) on the sputtering of cholesterol layers at equilibrium. At constant beam energies, the sputter rates appeared to be relatively independent of the cluster size. They also observed little change in the secondary ion spectrum between the studied cluster ions during depth profiling except that C_{60}^+ ions resulted in significantly greater damage.

Bich et al.[28] also analysed cholesterol in depth profiles from rat brain tissue sections but here the study uses 10 keV Ar_{1500}^+ ions incident at 45°. Good consistent profiles were observed through the tissue section. The migration of cholesterol to the surface was observed.

Due to the frequent occurrence of cholesterol in biological samples[29] and its tendency to segregate, it is important to characterize the cholesterol sputtering yields for argon cluster sputtering over a range of energy and cluster sizes so that a general description of the behaviour may be established. For the present study, thin layers of cholesterol were therefore deposited on cleaned Si wafers and initial depth profiles were made using 2.5 to 20 keV Ar_{1000}^+ and Ar_{5000}^+ at 45° incidence angle at room temperature. These showed anomalous effects and so further profiles were made using 10 and 20 keV $C_{60}^{+(+)}$ sputtering beams. These were good, as previous reports show, indicating that the films were coherent and the material condensed from evaporation had no degradation. Good profiles were then made by cooling the sample to -100 °C whilst profiling and finally, excellent profiles were obtained for cholesterol films deposited on amiodarone on the silicon wafer. These lead to an excellent description of the absolute yields and their temperature dependence through Seah's universal equation.[14]

EXPERIMENTAL

All samples were prepared on ~1 cm^2 pieces of UV/ozone-cleaned oxidized silicon substrates (University Wafer, Boston, MA, USA). Cholesterol and amiodarone hydrochloride (both from Sigma Aldrich) were deposited onto the wafers by thermal evaporation using an Edwards AUTO 306 vacuum coater (Edwards

Vacuum, Crawley, UK). The thickness of all films was determined using spectroscopic ellipsometry (Woollam M2000, J.A. Woollam Co., Lincoln, NE, USA).

For the reference spectra a small amount of cholesterol powder was dissolved in chloroform. A drop of the solution was then deposited on to a silicon substrate and evaporated in air.

Depth profiling analysis through the films were performed using a TOF-SIMS IV (ION-TOF GmbH, Münster, Germany). A temperature-controlled sample stage allowed temperatures to be set in the range -100 °C to 100 °C. The experiments were performed in a dual beam mode, where the mass spectrometer operates alternatingly between erosion cycles and mass spectra acquisition cycles. During the erosion cycle, either the $C_{60}^{+(+)}$ or Ar_n^+ ion beam was used to etch through the film at a larger area of at least 500 µm × 500 µm. Positive secondary ion spectra were collected between the erosion cycles from a central area within the etched crater (50 µm x 50 µm for $C_{60}^{+(+)}$ and 200 µm × 200 µm for Ar_n^+ experiments). This was done using a 25 keV Bi_3^+ ion beam. The Bi_3^+ ion current was at 0.1 pA or below. $C_{60}^{+(+)}$ depth profiles were acquired with two cluster energies 10 keV and 20 keV. Ar_n^+ experiments were done using cluster sizes of n = 1000, n = 2000 and n = 5000 at energy ranges from 2.5 to 20 keV. In all the experiments, the beam currents were set so that the ratio of beam current dose densities between the analytical beam (Bi_3^+) and the sputter beams ($C_{60}^{+(+)}$ and Ar_n^+) was at ~ 1 % or below to avoid altering the Ar sputtering yields. This allowed sufficiently high SIMS signal for good quality spectra, while keeping the impact of bismuth sputtering on such low level that it could be disregarded. Both cluster ion beams were at 45° to the surface normal.

RESULTS AND DISCUSSIONS

DEPTH PROFILES OF CHOLESTEROL ON SILICON USING Ar_n^+ AT ROOM TEMPERATURE

A typical positive secondary ion spectrum from a freshly deposited and dried droplet of cholesterol is shown in Figure 1. Cholesterol is represented by the peaks at 369 Da and 385 Da corresponding to $[M\text{-}OH]^+$ and $[M\text{-}H]^+$, respectively. To expand the abscissa, the peak at 754 Da for $[2M\text{-}H_2O\text{-}H]^+$ has been omitted but on this scale is significant but small at 32 counts. This spectrum is the same as that found throughout the present argon cluster depth profiles except as noted separately.

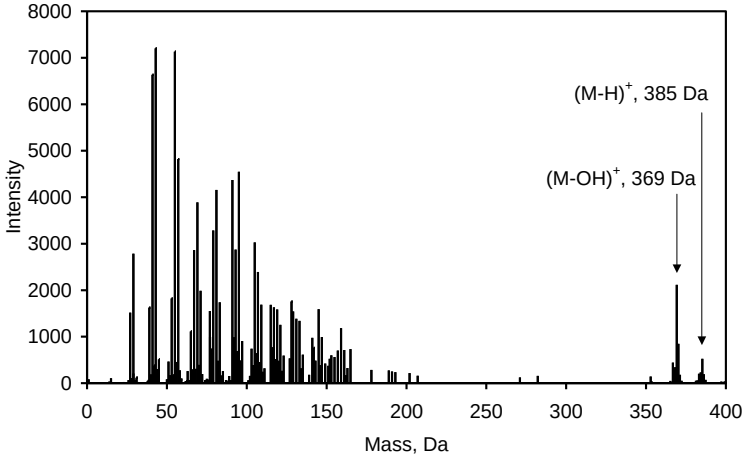

Figure 1. Cholesterol positive secondary ion spectrum after sputtering with 10 keV Ar_{1000}^+ and analysing with 25 keV Bi_3^+. The compositions of $[M\text{-}H]^+$ and $[M\text{-}OH]^+$ are $C_{27}H_{45}O^+$ and $C_{27}H_{45}^+$, respectively. The region with $[2M\text{-}H_2O\text{-}H]^+$ at 754 Da is omitted for clarity.

A typical depth profile for a 42 nm thick film, at room temperature and using 2.5 keV Ar_{1000}^+, is shown in Figure 2a for the fragments traditionally used to characterize cholesterol. It is clear that an approximate dose for the interface is somewhere in the range 0.85 to 1.3 ions/nm^2 leading to yield volumes of between 49 and 32 nm^3. This is useful but provides a dose range of ± 20% for sputtering the film and the

interfaces show a modest depth resolution based on the 16% to 84% width of 9 nm. The depth profiles for the other *E* and *n* settings have very different doses but are otherwise similar. However, these profiles are not as repeatable as one may expect. Occasionally, one or two steps or undulations are visible in the profile; those in the interface region degrading the depth resolution. We shall, for now, focus on the 2.5 keV Ar_{1000}^+ data since they typically illustrate many of the issues.

Figure 2b shows the total ion yield (TIY) profile and also that for $SiOH^+$ from the wafer with an oxide layer ~5 nm thick. The total ion yield is related to the sputtering yield[30] and the change of more than an order of magnitude around 1 ion/nm^2 emphasizes the great disparity of the sputtering yields of the organic layer and the inorganic substrate. However, there is a significant region in the doses between about 1.0 and 1.2 ions/nm^2 where the cholesterol intensity is at less than half and the bare wafer signal is also less than half.

Figure 2c shows the profiles for the series of secondary ion fragments from $C_4H_3^+$ to $C_4H_9^+$. It is clear that the more degraded peaks with greater hydrogen loss are relatively stronger at the interface. These degraded fragments may arise from a more degraded cholesterol residing at the interface or they may arise from a higher energy deposition density in the ion impact at the interface where the sputtering yield falls dramatically – the argon atoms largely bounce off the SiO_2, sputtering about 0.2 atoms per cluster: a rate less than one thousandth of that for cholesterol. The degraded product is expected to have a lower sputtering yield and, in the limit when all of the hydrogen is removed, the yield would be similar to that of silicon, some 3 orders of magnitude lower than that of cholesterol.[14] If we focus on the mid-point of the interface at 1.2 ions/nm^2, the relative intensities of the fragments here to the intensities averaged for doses up to 0.6 ions/nm^2 are shown in Figure 2d. The profiles for $C_4H_9^+$ (m/z = 57) in Figure 2c are very similar to those for the TIY in Figure 2b. The difference between the curves in Figure 2c show the degraded material starts at a dose of 0.6 ions/nm^2, reaches a peak at 1.2 ions/nm^2 and then persists to higher doses.

It will be noticed in Figure 2c that the profiles for $C_4H_3^+$ and $C_4H_4^+$ appear to proceed at significant fractional intensity into the Si. These are actually very weak peaks in the spectrum shown in Figure 1 since the argon clusters cause little degradation. However, these small peaks persist at higher doses as they have a low sputtering yield.

We need to know if the apparently damaged material at the interface arises from the sample preparation, e.g. catalytic decomposition of the cholesterol at the hydrated silicon surface, or the sputtering conditions. Figure 2d resembles the plots customarily made in studies in G-SIMS[31-33] where this result would be obtained for the ratio of spectra using a higher energy deposition density condition to one of lower energy density. Clearly, the damage at the interface is consistent with a higher energy deposition density from the ion impact.

It appears, therefore, that at room temperature the profiles are somewhat variable and that, at the interface with the Si wafer, significant degradation occurs. After profiling these samples, the films were studied by optical microscopy and it was clear that, in the film area exposed to the instrumental environment, but outside the sputtered crater, the film had changed morphology. The same film under the sample holder mask was unchanged, indicating that it was not a simple issue of the vacuum or of the wafer temperature. It was clear that radiation in the vacuum environment, other than the direct sputtering and analysis ion beams had led to significant film restructuring. Although this would lead to poor depth resolution, as indeed seen in Figure 2, it would not necessarily alter the sputtering yield measurement. For example, if there were no effects other than simple sputtering, a layer that is rearranged into an area covering 50% of the surface, but was twice as thick, would take twice as long to sputter through

as the same material at 100% coverage – but the signal would be half as strong. If the rearrangement led to a more complex distribution of thicknesses, the integral of the area under the curve for the normalised yield would then deliver precisely the dose required to remove the same film unreconstructed. It is easy to calculate this from the profiles and this would be our procedure if there were no alternative. AFM studies of the films, as exampled in Figure 3, indicate that the film is restructuring and de-wetting. This was surprising since C_{60}^+ profiling had been successful as shown in the next section. We shall return to these AFM measurements later.

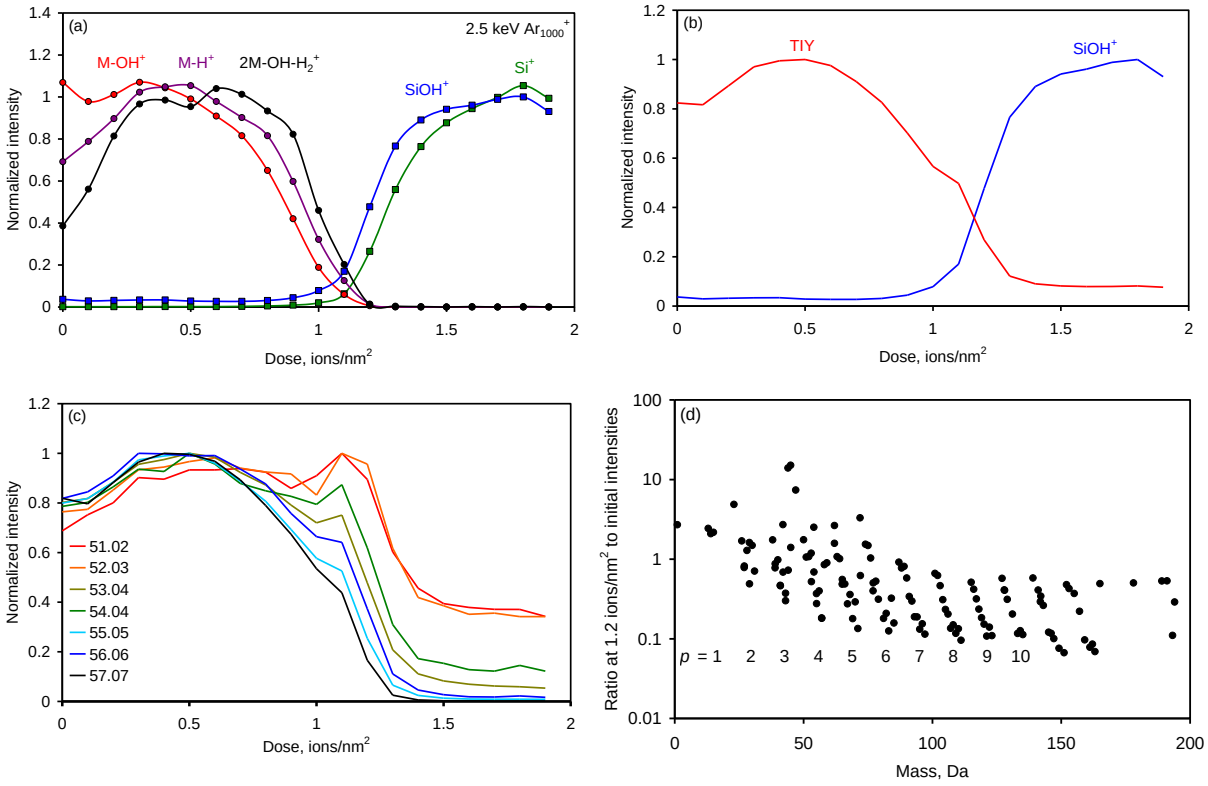

Figure 2. Profile for a 42 nm thick cholesterol film on silicon sputtered by 2.5 keV Ar_{1000}^+ and analysed by 25 keV Bi_3^+ at room temperature, (a) profile showing the molecular and substrate normalised intensities, (b) the total ion yield and $SiOH^+$ normalised intensities, (c) intensities for the $C_4H_3^+$ to $C_4H_9^+$ ion fragment series with masses shown in Da, and (d) the ratio of intensities at 1.2 ions/nm^2 for fragments C_pH_r with p increasing from 1 to 12 and r typically ranging from p to $2p$, compared with their intensities in pure cholesterol.

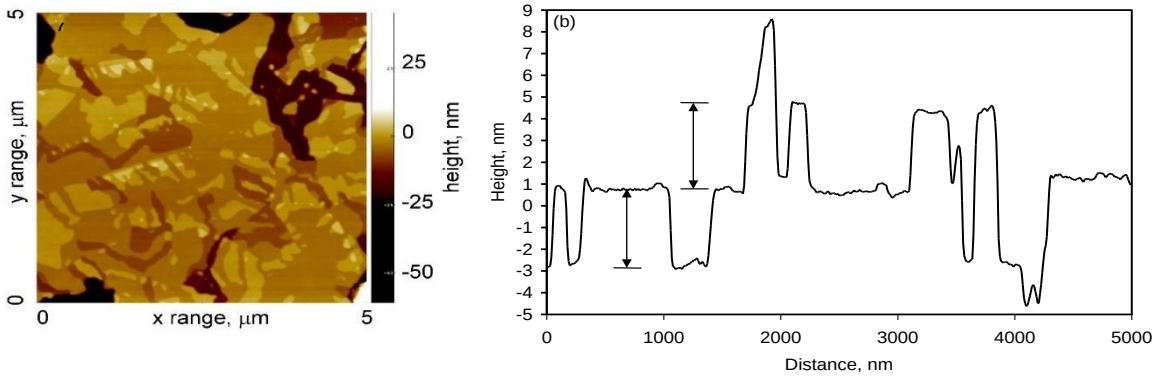

Figure 3. (a) AFM image of the 42 nm thick cholesterol film on silicon exposed to radiation in the SIMS instrument, such as light and low energy electrons but outside the area of the sputtering and analysis ion beams. The field of view is 5 µm by 5 µm. (b) x-line trace at y = 2.4 µm showing the bilayer steps (indicated by arrows).

DEPTH PROFILES OF CHOLESTEROL ON SILICON USING C_{60}^+ IONS AT ROOM TEMPERATURE

Profiles were also measured for similarly produced films of cholesterol using 10 keV C_{60}^+ and 20 keV C_{60}^{++}. Figure 4 shows the profile for an 86 nm film profiled with 10 keV C_{60}^+ and analysed using 25 keV Bi_3^+ ions. The profile is now much as expected. There is a rapid fall at the start as C_{60}^+ debris is incorporated and the cholesterol damage is equilibrated, followed by a good plateau and then, at the end, a sharp interface. The depth resolution from the $SiOH^+$ signal is around 9% or 7.5 nm. The increase before the interface may arise from an enhanced sputtering yield there since the bonding of the cholesterol to the Si wafer is weaker than the bonding to itself – this is the driving force for the film restructuring and de-wetting, as shown in Figure 3. Alternatively, or as well, the increase may either arise from the higher energy deposition density at the interface with the low yield of the substrate or from enhanced ionisation at the oxide surface. For determining the sputtering yield, we take the dose to bring the $SiOH^+$ signal to 50% of its maximum. By averaging results for both positive and negative secondary ion yields, we find Y (10 keV) = 105.5 $\pm$ 4.0 nm^3 and Y (20 keV) = 220.9 $\pm$ 0.3 nm^3. Using any other peak does not change these values significantly. It is clear that the cholesterol film has not restructured during profiling or the 7.5 nm depth resolution and repeatable data would not be attained.

In sputtering with $C_{60}^{+(+)}$, carbon atoms are incorporated into the surface, changing the sample there and possibly forming a thin skin of higher melting point[34] at the surface (as on paint or custard). The raised melting temperature arises from the loss of simple hydrogen bonding between the melting entities. This will inhibit the film break up and, here, has led to the better C_{60}^+ profile compared with Ar_n^+. The Ar_n^+ will leave the surface very clean and labile. To reduce the possibility of film restructuring, the Ar_n^+ measurements were now repeated for films cooled to -100 °C prior to any exposure to radiation.

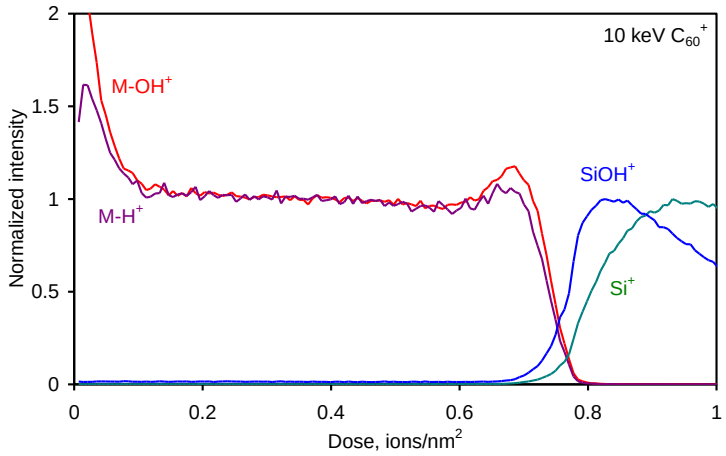

Figure 4. Profile of an 86 nm thick cholesterol film on silicon sputtered by 10 keV C_{60}^+ and analysed by 25 keV Bi_3^+ at room temperature showing the molecular and substrate normalised intensities.

DEPTH PROFILES OF CHOLESTEROL ON SILICON USING Ar_n^+ AT - 100 °C

To obtain a greater degree of accuracy, the films here are 145.5 nm thick. Both the increase in thickness and the lower temperature are expected to inhibit film restructuring. The profiles using Ar_n^+ now look closer to those for C_{60}^+ at room temperature than those of Ar_n^+ at room temperature. Figure 5a shows the result for 2.5 keV Ar_{1000}^+ with a depth resolution for the Si^+ profile of 9 nm. Repeat profiles are now consistent.

Figure 5b is the counterpart of Figure 2c for the series $C_4H_3^+$ to $C_4H_9^+$. We see an identical behaviour at the interface, to that at room temperature, with the more degraded component being strongest at the interface. However, the effect is weaker although the depth resolution for this thicker film is the same 9 nm as that at room temperature. There is a clear peak in all intensities prior to the interface and at that peak we see the inverse of the result shown in Figure 2d. Instead of being weakest, the $C_4H_{10}^+$ is strongest and $C_4H_3^+$ is weakest. This shows that prior to the interface the cholesterol is sputtered more easily and this may simply be that there is better ordering of the initial layers deposited. The reduced mobility of the film has been strongly beneficial overall. The equivalent plot of data, as in Figure 2d at the interface, is reduced by a factor of more than 5 with a similar, but inverted plot to that at the peak (at a dose of ~8 ions/nm^2).

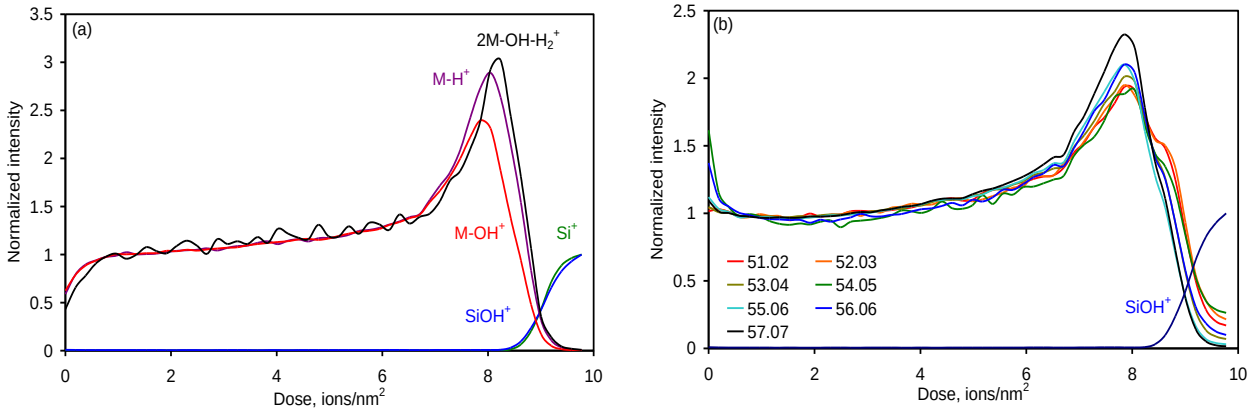

Figure 5. Profile showing intensities normalised to those at low dose of a 145.5 nm thick cholesterol film on silicon sputtered by 2.5 keV Ar_{1000}^+ cluster ions and analysed by 25 keV Bi_3^+ at -100º C, (a) profile showing the molecular and substrate normalised intensities, (b) intensities for the $C_4H_3^+$ to $C_4H_9^+$ ion fragment series with masses shown in Da as in Figure 2c.

From these data, using the rise in the $(SiOH)^+$ signal, we may directly calculate the sputtering yield volumes for Ar_n^+ for n = 1000 and 5000 and 2500 ≤ E ≤ 20000 eV incident at 45° to the surface normal, as shown in Figure 6. These are for cholesterol at -100 °C and we do know that the sputtering yields will rise with temperature although, at this stage, we do not know the magnitude of this effect. The data are plotted as Y/n in nm^3 versus E/n in eV together with the fit for equation (1) with B = 0.0045 nm^3, A = 0.48 eV and q = 1.95. The data fit equation (1) with a scatter of 11%. This excellent result is close to that expected but may be slightly worse than the 7 to 8% seen by Seah[14] as a result of the changing yield at the interface with the silicon wafer. To the top right, the room temperature $C_{60}^{+(+)}$ data are added. In Figure 6, the $C_{60}^{+(+)}$ data are plotted as Y/n and E/n, although Delcorte et al.,[35] from molecular dynamics simulations, would predict the results for Ar_n^+ and $C_{60}^{+(+)}$ ions to be consistent when plotted as Y/N versus E/N where N is the number of nucleons on the sputtering particle, not the number of atoms. If this were done, the $C_{60}^{+(+)}$ values would shift, relative to the Ar_n^+ values, by a factor (40/12) on both axes. The line in this region is essentially at unity gradient and so the quality of the fit would be unchanged. That the sputtering yield data for $C_{60}^{+(+)}$ at room temperature fit the data for Ar_n^+ at –100 °C is surprising since the degradation caused by the $C_{60}^{+(+)}$ is expected to reduce the yield but, as we shall see, the Ar_n^+ data at -100 °C are a factor of approximately 1.8 times lower than at room temperature.

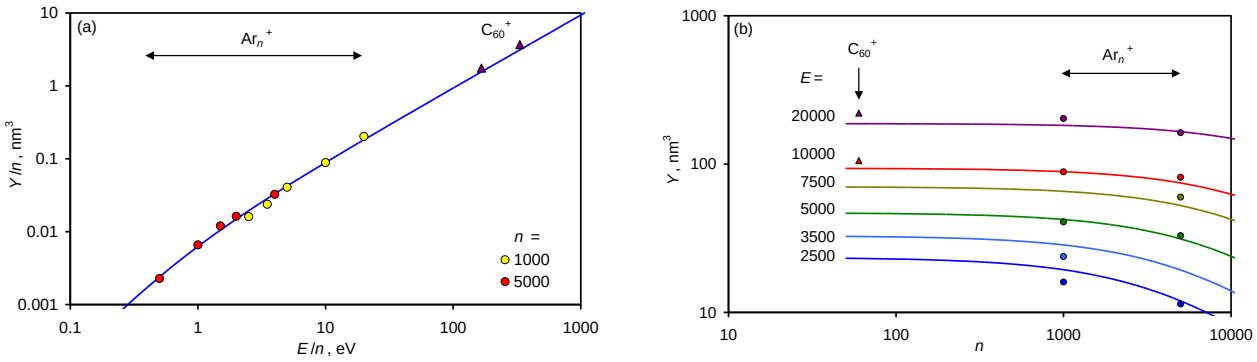

Figure 6. The sputtering yields of cholesterol for both Ar_n^+ and $C_{60}^{+(+)}$ sputtering with the fit of equation (1) with B = 0.0045 nm^3, A= 0.48 eV and q = 1.95. The rms scatter of the data about the fitted curve(s) is 11%. The Ar_n^+ data are for -100 ºC and the $C_{60}^{+(+)}$ data are for room temperature. (a) The Y/n vs E/n Universal Plot and (b) the Y vs n plot.

CHOLESTEROL ON SILICON AT ROOM TEMPERATURE

Although we have the sought-after sputtering yield volumes, the results for sputtering at room temperature deserve closer attention since many SIMS and other studies are conducted in vacuum at room temperature and organic molecules like cholesterol are being increasingly studied. The melting point of anhydrous cholesterol is often given as 148 °C but Loomis et al.[36] measure the crystalline to liquid transition at 151 °C. They also show that cholesterol monohydrate converts to anhydrous cholesterol at 86 °C and that anhydrous cholesterol will not hydrate at or below 90% relative humidity at 22 °C in 120 hours. It is therefore safe to assume that we are dealing with anhydrous cholesterol and that it should be stable at room temperature. Good profiles are made at room temperature for Irganox 1010,[8, 37] NPB[15] and the polymers PS[7, 38] and PMMA[38, 39] whose melting points are 118 °C, 277 °C, 240 °C and 160 °C, respectively and so, from the melting temperature, one would not expect room temperature to be excessive.

Line traces across the AFM image of Figure 3 show clear plateaus and sharp steps with the step edges sharper than the 10 nm of the image resolution. Measurements of many steps, as exampled in Figure 3b, give a step height of 3.6 ± 0.2 nm with, occasionally, twice or four times this value where the edges of layers coincide. At the top of Figure 3a are two areas at heights of about -51 nm, probably indicating the bare substrate. There are no steps of 1.8 nm. Shieh et al.[40] note that anhydrous cholesterol forms a triclinic crystal structure with 8 independent molecules per cell. Four of the molecules are shown in Figure 7a. The -OH groups bond the molecules end-to-end with a total length of 3.4 nm, very close to the measured step heights. Loomis et al.[36] note that cholesterol and cholesterol monohydrate will form smectic liquid crystal bilayers of molecules end-to-end. This is shown in Figure 7b. The structures of cholesterol and cholesterol monohydrate are very similar. Nes[41] in his review shows the maximum length of the cholesterol molecule as 1.9 nm. Studies of cholesterol monohydrate by Aberdan and Swift,[42] using AFM, show films with steps with the smallest feature about 3.4 nm which they interpret with structures much as in Figure 7.

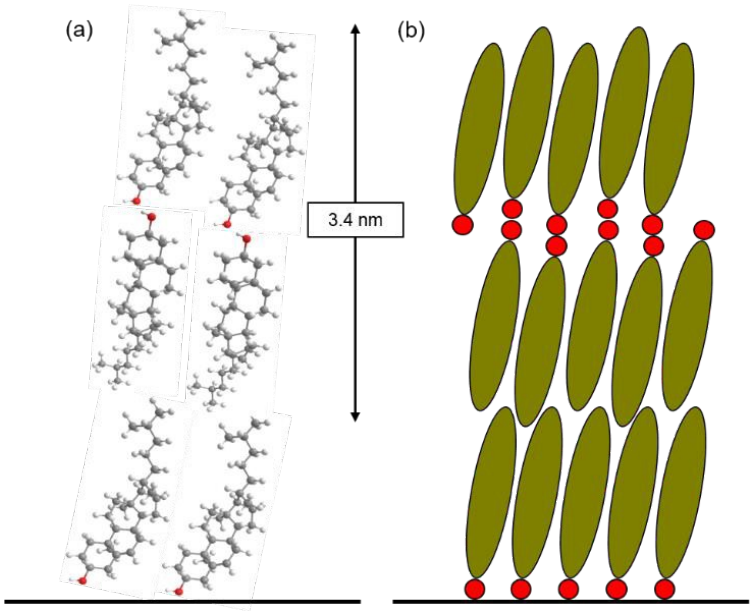

Figure 7. (a) The structure of anhydrous cholesterol showing four of the molecules in the unit cell. The cell length with the two molecules with their –O atom shown by the red sphere and the adjacent hydrogen atom shown by the white sphere is 3.4 nm. (b) Schematic of the layer structure.

It therefore seems very likely that bilayers have formed as a result of radiation or field-enhanced diffusion at or near room temperature, disrupting the deposited smooth film. Loomis,[36] Hsu and Nordman[43] and Bach and Wachtel[44] and others note that, around 37 °C, anhydrous cholesterol undergoes a polymorphic transition from one triclinic space group to another in which the number of molecules in the cell doubles and length of the a-axis is doubled, i.e. there is a bit of shuffling and rotation of the molecules about their long axis but the essential bilayer structure and the associated step height are unchanged. This phase transition may be sufficient to aid the movement of molecules to break up the film that is stable in air at room temperature.

This restructuring process may enhance the sputtering yield since the ordering may allow the molecules to be more easily separated. The enhancement would depend on the degree of ordering into bilayers. In most profiles, analysis of the ratio of the intensity for the dimer $[2M\text{-}H_2O\text{-}H]^+$ to the monomer $[M\text{-}OH]^+$ shows a linear increase as the interface is approached, starting 20 nm from the interface and reaching a factor of 3 or more as the last fragments are removed. This may indicate that, in most profiles, the ordering into dimer layers is strong at the Si surface but becomes disordered as the layer thickens, with full disorder at 20 nm thickness. To test this, we next study cholesterol with an inter-layer covering the silicon substrate.

CHOLESTEROL ON AMIODARONE ON SILICON AT VARIOUS TEMPERATURES

In the above, we have established the sputtering yield of cholesterol from silicon wafers at -100 °C as shown in Figure 6 and that the yield at room temperature is approximately 1.8 times higher. It is not clear yet if these yields are significantly affected by the possible ordering in the structures made on silicon that may be different from those on organic substrates. We therefore study a 67.9 nm cholesterol film deposited on 37 nm of amiodarone on silicon using 5 keV Ar_{2000}^+ at temperatures between -50 °C and 75 °C. A profile for the cholesterol layer is shown in Figure 8. The peak and interfacial degradation have now gone and the profile is well behaved. Many peaks follow the same profile as that shown here at -50 °C. Figure 8 shows example data for a molecular and a highly degraded peak. Both, and all peaks studied, show the same interface position and depth resolution of 8.7 nm. The effects shown in Figures 2c and d do not occur, nor the enhancement of the $[2M\text{-}H2O\text{-}H]^+$ compared with $[M\text{-}OH]^+$ seen in the

final 20 nm at the interface for layers on silicon. The earlier effects attributed to higher energy deposition density and/or weakened bonding or enhanced ionisation at the interface are no longer apparent since those causes have been removed by the amiodarone inter-layer.

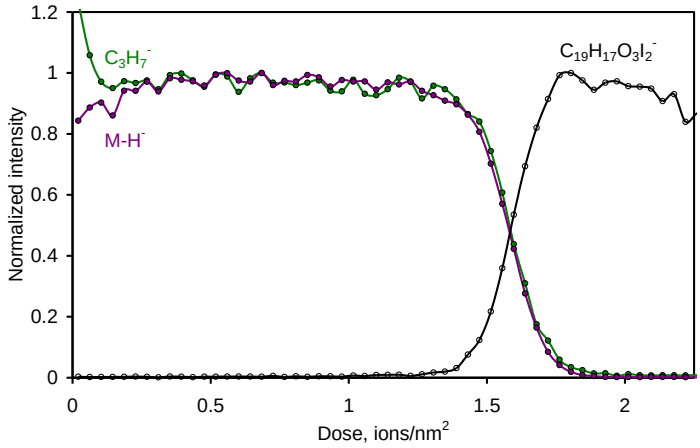

Figure 8. Normalised profile for a 67.9 nm film of cholesterol ($[M-H]^-$ and $[C_3H_7]^-$ hydrocarbon ion) on 37 nm of amiodarone ($[C_{19}H_{17}O_3I_2]^-$)sputtered using 5 keV Ar_{2000}^+ ions and analysed by 25 keV Bi_3^+ at -50° C

From Figure 8 we may deduce the sputtering yield and, using the values of *B* and *q* determined earlier, the value of *A*. Measurements for many temperatures give the green data for *A* shown in Figure 9. The value of *A* falls with temperature fairly smoothly, supporting the 1.8 times increase at room temperature mentioned earlier shown by the red data. The yields were measured up to 75 °C, but at that temperature significant profile distortion had occurred. At 50 °C the profiles were useful but the depth resolution had degraded to 20 nm. At room temperature the depth resolution was 9.8 nm and the profiles were similar to that shown in Figure 8 although with some minor differences. These differences persisted down to -25 °C.

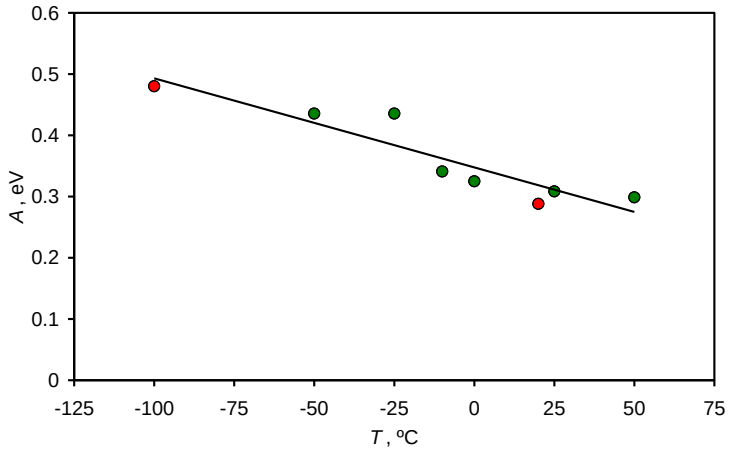

Figure 9. Evaluation of the parameter *A*, eV, from equation (1) with *B* = 0.0045 nm^3 and *q* = 1.95 as a function of temperature, for cholesterol on (red symbols) silicon and (green symbols) amiodarone.

CONCLUSIONS

The sputtering yield of cholesterol has been measured on samples with temperature reduced to -100 °C. This enables measurements to be made at various energies and cluster sizes. The results fit, within a scatter of 11%, the Universal Equation for sputtering yields, equation (1), with *B* = 0.0045 nm^3, *A* = 0.48

eV and q = 1.95. Measurements recorded at room temperature show a lack of repeatability in the profile curves, some showing downward steps at the broad interface. This broad interface shows significant intensities of the more degraded fragments. The sputtering yields may be obtained and show an elevated yield of 1.8 times those at -100 °C, a factor that could arise partly from the change in structure of the layer and/or partly the higher temperature. AFM measurements show that the layer exposed in the SIMS instrument at room temperature can reconstruct from a smooth layer to one composed of parts of layers of 3.6 ± 0.2 nm thickness interpreted as bilayers of cholesterol molecules standing inclined at a small angle to the surface normal. This structure may enhance the sputtering yield and leads to a poorer quality depth profile. This arises at room temperature as a result of radiation or field enhanced diffusion in the vacuum of the SIMS instrument and does not occur when stored in air at room temperature. C_{60}^+ depth profiles at room temperature seem free from this restructuring maybe as a result of the carbon deposition and damaged material in the surface layer. The C_{60}^+ sputtering yields are a factor of 1.6 lower than those for Ar_n^+ at room temperature. Profiles for layers deposited on amiodarone instead of silicon are well behaved for all secondary ions with a yield steadily rising with temperature. This is interpreted as an effective reduction in the A energy of the Universal Equation as the temperature rises.

Cholesterol is one of the most abundant and most important lipid molecules in mammalian organisms. It is important, when analysing with SIMS that its mobility is recognised as well as the unwanted effects of temperature, vacuum or radiation within the instrument. The substrate too can be an issue and silicon wafers should be covered by an organic interlayer. Here, an amiodarone interlayer is shown to remove the unwanted effects and leads to profiles without anomalies. With the technology developments, the number of studies utilising high-resolution imaging and 3D analysis of tissues and cells, including subcellular 3D imaging, is rapidly growing. As the resolution of the analysis increases, removal of these unwanted effects becomes more and more critical.

CORRESPONDING AUTHOR

E-mail: paulina.rakowska@npl.co.uk

NOTES

The authors declare no competing financial interest.

ACKNOWLEDGEMENT

The authors would like to thank C. A. Clifford for the AFM measurements. This work forms part of the 3D NanoSIMS project in the Chemical and Biological programme of the National Measurement System of the UK Department of Business, Innovation and Skills.

REFERENCES

1. Y. Sun, P. Sukumaran, A. Varma, S. Derry, A. E. Sahmoun and B. B. Singh, *Biochim. Biophys. Acta, Mol. Cell Res.*, 2014, **1843**, 1839-1850.
2. S. Yue, J. Li, S. Y. Lee, H. J. Lee, T. Shao, B. Song, L. Cheng, T. A. Masterson, X. Liu, T. L. Ratliff and J. X. Cheng, *Cell Metab.*, 2014, **19**, 393-406.
3. L Stryer, J. M. Berg and J. L. Tymoczko, *Biochemistry* W. H. Freeman, New York, 5th edn., 2002.
4. F. R. Maxfield and I. Tabas, *Nature*, 2005, **438**, 612-621.
5. A. Lazar, C. Bich, M. Panchal, N. Desbenoit, V. Petit, D. Touboul, L. Dauphinot, C. Marquer, O. Laprévote, A. Brunelle and C. Duyckaerts, *Acta Neuropathol.*, 2013, **125**, 133-144.
6. J. Matsuo, S. Ninomiya, Y. Nakata, Y. Honda, K. Ichiki, T. Seki and T. Aoki, *Appl. Surf. Sci.*, 2008, **255**, 1235-1238.
7. D. Rading, R. Moellers, H. G. Cramer and E. Niehuis, *Surf. Interface Anal.*, 2013, **45**, 171-174.
8. E. Niehuis, R. Möllers, D. Rading, H. G. Cramer and R. Kersting, *Surf. Interface Anal.*, 2013, **45**, 158-162.

9. M. P. Seah, *Surf. Interface Anal.*, 2007, **39**, 890-897.
10. M. K. Passarelli, C. F. Newman, P. S. Marshall, A. West, I. S. Gilmore, J. Bunch, M. R. Alexander and C. T. Dollery, *Anal. Chem.*, 2015, **87**, 6696-6702.
11. E. Niehuis, R. Moellers, D. Rading and P. Bruener, *Surf. Interface Anal.*, 2014, **46**, 70-73.
12. M. P. Seah, S. J. Spencer, R. Havelund, I. S. Gilmore and A. G. Shard, *Analyst*, 2015, **140**, 6508-6516.
13. M. K. Passarelli and A. G. Ewing, *Curr. Opin. Chem. Biol.*, 2013, **17**, 10.1016/j.cbpa.2013.1007.1017.
14. M. P. Seah, *J. Phys. Chem. C*, 2013, **117**, 12622-12632.
15. M. Holzweber, A. G. Shard, H. Jungnickel, A. Luch and W. E. S. Unger, *Surf. Interface Anal.*, 2014, **46**, 936-939.
16. M. P. Seah, *Surf. Interface Anal.*, 2015, **47**, 169-172.
17. H. Nygren, P. Malmberg, C. Kriegeskotte and H. F. Arlinghaus, *FEBS Lett.*, 2004, **566**, 291-293.
18. P. D. Piehowski, A. J. Carado, M. E. Kurczy, S. G. Ostrowski, M. L. Heien, N. Winograd and A. G. Ewing, *Anal. Chem.*, 2008, **80**, 8662-8667.
19. S. Rabbani, A. M. Barber, J. S. Fletcher, N. P. Lockyer and J. C. Vickerman, *Anal. Chem.*, 2011, **83**, 3793-3800.
20. H. Nygren, K. Börner, P. Malmberg and B. Hagenhoff, *Appl. Surf. Sci.*, 2006, **252**, 6975-6981.
21. T. B. Angerer, M. Dowlatshahi Pour, P. Malmberg and J. S. Fletcher, *Anal. Chem.*, 2015, **87**, 4305-4313.
22. E. A. Jones, N. P. Lockyer and J. C. Vickerman, *Anal. Chem.*, 2008, **80**, 2125-2132.
23. E. A. Jones, N. P. Lockyer and J. C. Vickerman, *Applied Surface Science*, 2006, **252**, 6727-6730.
24. P. Sjövall, B. Johansson and J. Lausmaa, *Appl. Surf. Sci.*, 2006, **252**, 6966-6974.
25. J. Vickerman and N. Winograd, in *Cluster Secondary Ion Mass Spectrometry*, John Wiley & Sons, Inc., 2013, DOI: 10.1002/9781118589335.ch8, pp. 269-312.
26. J. Kozole, D. Willingham and N. Winograd, *Appl. Surf. Sci.*, 2008, **255**, 1068-1070.
27. K. Shen, D. Mao, B. J. Garrison, A. Wucher and N. Winograd, *Anal. Chem.*, 2013, **85**, 10565-10572.
28. C. Bich, R. Havelund, R. Moellers, D. Touboul, F. Kollmer, E. Niehuis, I. S. Gilmore and A. Brunelle, *Anal. Chem.*, 2013, **85**, 7745-7752.
29. J. S. O'Brien and E. L. Sampson, *Journal of Lipid Research*, 1965, **6**, 537-544.
30. M. P. Seah, R. Havelund and I. S. Gilmore, *J. Phys. Chem. C*, 2014, **118**, 12862-12872.
31. I. S. Gilmore and M. P. Seah, *Appl. Surf. Sci.*, 2000, **161**, 465-480.
32. I. S. Gilmore, F. M. Green and M. P. Seah, *Surf. Interface Anal.*, 2007, **39**, 817-825.
33. F. M. Green, F. Kollmer, E. Niehuis, I. S. Gilmore and M. P. Seah, *Rapid Commun. Mass Spectrom.*, 2008, **22**, 2602-2608.
34. J. B. Austin, *Journal of the American Chemical Society*, 1930, **52**, 1049-1053.
35. A. Delcorte, B. J. Garrison and K. Hamraoui, *Anal. Chem.*, 2009, **81**, 6676-6686.
36. C. R. Loomis, G. G. Shipley and D. M. Small, *J. Lipid Res.*, 1979, **20**, 525-535.
37. A. G. Shard, R. Havelund, M. P. Seah, S. J. Spencer, I. S. Gilmore, N. Winograd, D. Mao, T. Miyayama, E. Niehuis, D. Rading and R. Moellers, *Anal. Chem.*, 2012, **84**, 7865-7873.
38. V. Cristaudo, C. Poleunis, B. Czerwinski and A. Delcorte, *Surf. Interface Anal.*, 2014, **46**, 79-82.
39. K. Ichiki, PhD Thesis, Kyoto University, 2012.
40. H. S. Shieh, L. G. Hoard and C. E. Nordman, *Nature*, 1977, **267**, 287-289.
41. W. D. Nes, *Chem. Rev.*, 2011, **111**, 6423-6451.
42. R. S. Abendan and J. A. Swift, *Langmuir*, 2002, **18**, 4847-4853.
43. L. Hsu and C. Nordman, *Science*, 1983, **220**, 604-606.
44. D. Bach and E. Wachtel, *Biochim. Biophys. Acta, Biomembr.*, 2003, **1610**, 187-197.